

Study of a Convergent Subsetized List-mode EM Reconstruction Algorithm

A. Rahmim¹, T. J. Ruth², and V. Sossi¹

¹Department of Physics and Astronomy, University of British Columbia, Vancouver, BC Canada

²UBC/Triumf, Vancouver, BC Canada

E-mail: rahmim@physics.ubc.ca, truth@triumf.ca, and vesna@physics.ubc.ca

Abstract— We have implemented a convergent subsetized (CS) list-mode reconstruction algorithm, based on previous work [1]–[3] on complete-data OS-EM reconstruction. The first step of the convergent algorithm is exactly equivalent (unlike the histogram-mode case) to the regular subsetized list-mode EM algorithm, while the second and final step takes the form of additive updates in image space. A hybrid algorithm based on the ordinary and the convergent algorithms is also proposed, and is shown to combine the advantages of the two algorithms: it is able to reach a higher image quality in fewer iterations while maintaining the convergent behavior, making the hybrid approach a good alternative to the ordinary subsetized list-mode EM algorithm. Reconstructions using various LOR-driven projection techniques (Siddon method, trilinear and bilinear interpolation) were considered and it was demonstrated that in terms of FWHM, the Siddon technique is inferior to the other two algorithms, with the bilinear interpolation technique performing nearly similarly as the trilinear while being considerably faster.

I. INTRODUCTION

Since the introduction of the ordered subset (OS) EM algorithm for histogram-mode emission tomography by Hudson *et al.* [4], there has been considerable interest in accelerated image reconstruction techniques. The OS principle (using a subset of the measurement data for each update instead of the total data set) has subsequently been used to yield other reconstruction algorithms, such as the rescaled block-iterative (RBI) EMLL algorithm [5], [6], the OS separable paraboloidal surrogates (OS-SPS) method [7], and list-mode EM reconstruction [8], [9].

Such OS algorithms, however, are *not* convergent in general, and instead result in limit cycles. There has been interest by different research groups in deriving provably convergent versions of the fast OS methods. In [10], an alternate algorithm termed row-action maximum likelihood algorithm (RAMLA) was proposed along with a convergence proof. The authors have also introduced the block sequential regularized EM (BSREM) algorithm, which extends the RAMLA approach to the case of maximum a posteriori (MAP) reconstruction [11]. Two types of globally convergent relaxed ordered subsets algorithms were also presented in [12]: one by modifying the BSREM algorithm to yield an algorithm convergent under more realistic assumptions, and the other by relaxing the OS separable paraboloidal surrogates (OS-SPS) method. In [1], [2], Hsiao

et al. derived a new convergent complete data ordered subsets algorithm for histogram-mode EM reconstruction (C-OSEM). They have shown that the proposed algorithm monotonically decreases the complete data objective function, and furthermore demonstrated that the solution converges to the maximum of the log-likelihood objective function. This algorithm has the advantage that it does not involve any relaxation schedule. Furthermore, it can be extended to list-mode reconstruction (Sec. II) which we have explored and investigated in this work. Meanwhile, we have also investigated effects of various interpolation techniques (as used in the forward- and back-projection operations) on reconstructed image qualities (Sec. III).

II. ACCELERATED EM RECONSTRUCTION

A. Ordinary Subsetized List-Mode EM Algorithm

The list-mode EM algorithm can be accelerated by subdividing the list-mode data into segments that span a fraction of the total duration of the data. Dividing the data space into L subsets, we use S_l to denote the l th list-mode subset ($l=1\dots L$). We use $\lambda_j^{m,l}$ to denote the image estimate at voxel j at the m th iteration and l th subset. The subsetized list-mode expectation maximization algorithm (which we shall refer to as the S-LMEM algorithm) is then given by [13]:

$$\lambda_j^{m,l} = \frac{\lambda_j^{m,l-1}}{\sum_{i=1}^I p_{ij}} \sum_{k \in S_l} p_{i_k j} \frac{1}{\sum_{b=1}^J p_{i_k b} \lambda_b^{m,l-1}} \quad (1)$$

where i_k refers to the LOR along which the k th event is detected, and p_{ij} is the probability of an emission from voxel j being detected along LOR i .

Starting from first principles and using the complete data approach as in [1], [2], Khurd and Gindi [3] have been able to derive a convergent subsetized list-mode EM reconstruction algorithm. The authors have subsequently tested the convergence and speed-up achieved by the algorithm using simulated SPECT data. In what follows, we show in detail a derivation of the same algorithm using an approach based on re-visiting the histogram-mode technique. We go on to present an intuitive picture of how the algorithm proceeds using additive updates in image space.

B. Convergent Histogram-mode OS-EM Reconstruction

In histogram-mode reconstruction, dividing the data space into L LOR-based subsets, S_l is used to denote the l th histogram-mode subset ($l=1\dots L$). The C-OSEM can then be written in the form [1], [2]:

$$C_{ij}^{m,l} = n_i \frac{p_{ij} \lambda_j^{m,l-1}}{\sum_{b=1}^J p_{ib} \lambda_b^{m,l-1}}, \forall i \in S_l \quad (2)$$

$$\lambda_j^{m,l} = \frac{1}{\sum_{i=1}^I p_{ij}} \left[\sum_{s=1}^l \sum_{i \in S_s} C_{ij}^{m,s} + \sum_{s=l+1}^L \sum_{i \in S_s} C_{ij}^{m-1,s} \right] \quad (3)$$

where one sets $\lambda_j^{m,0} = \lambda_j^{m-1,L}$ at the beginning of each iteration, while using some initialization for $C_{ij}^{0,s}$ values. In place of the update Eq. (3), the ordinary OSEM algorithm performs the following

$$\lambda_j^{m,l} = \frac{1}{\sum_{i \in S_l} p_{ij}} \sum_{i \in S_l} C_{ij}^{m,l} \quad (4)$$

Thus, we see that the C-OSEM algorithm is different from the ordinary OSEM in that calculation of image updates at every subset (numerator of Eq. 3) is *not* limited to C_{ij} values for LORs in that subset only: this explains why the sensitivity correction factors (denominator of Eq. 3) include back-projection from *all* the LORs. Meanwhile, at any subset l , values of C_{ij} are *updated only* for LORs $i \in S_l$: this explains why the update image at each subset can be computed nearly as fast as that of regular OSEM.

C. Convergent Subsetized List-mode EM Algorithm

Similar issues, as in the OSEM algorithm, are present in subsetized list-mode reconstruction, and the proposed S-LMEM algorithm results in non-converging (e.g. limit cycles) behavior, as reported in Sec. V. Using transformations as in [8], one may extend the histogram-mode formulation presented in II-B into list-mode reconstruction. By defining list-mode subsets as event-based subsets, as compared to LOR-based subsets in histogram-mode reconstruction, and replacing the summations over the LORs by summations over the events, while replacing n_i in Eq. (2) by the numeral 1, it can be shown that one arrives at the following list-mode reconstruction update equations:

$$\tilde{\lambda}_j^{m,l} = \frac{\lambda_j^{m,l-1}}{\sum_{i=1}^I p_{ij}} \sum_{k \in S_l} p_{ikj} \frac{1}{\sum_{b=1}^J p_{ikb} \lambda_b^{m,l-1}} \quad (5)$$

$$\lambda_j^{m,l} = \sum_{s=1}^l \tilde{\lambda}_j^{m,s} + \sum_{s=l+1}^L \tilde{\lambda}_j^{m-1,s} \quad (6)$$

where $\tilde{\lambda}_j^{m,l}$ is an *intermediate* image vector produced by the first update Eq. (5), subsequently used by Eq. (6) to arrive at the overall image estimate $\lambda_j^{m,l}$. The initialization $\tilde{\lambda}_j^{0,s} = 1$ will be imposed for all s , while setting $\lambda_j^{m,0} = \lambda_j^{m-1,L}$ at the beginning of each iteration.

As shown in Eq. (6), the algorithm takes the form of additive updates in image-space, in that upon arriving at any subset l ,

the intermediate image updates which have been previously calculated for other subsets $\{\forall s | s \neq l\}$ are added to the update $\tilde{\lambda}_j^{m,l}$ calculated for the current subset l . We shall refer to this approach as the convergent subsetized list-mode EM (CS-LMEM) algorithm. We also note that it is easy to show that:

$$\lambda_j^{m,l} = \lambda_j^{m,l-1} + \tilde{\lambda}_j^{m,l} - \tilde{\lambda}_j^{m-1,l} \quad (7)$$

From this observation, it follows that by keeping track of the values of $\lambda_j^{m,l-1}$ and the values of $\tilde{\lambda}_j^{m,l}$ for all subsets $S_l, l=1\dots L$, values of $\lambda_j^{m,l-1}$ can be recursively updated according to the above relation. This makes the calculation of image updates using the CS-LMEM algorithm nearly as fast as the regular S-LMEM algorithm.

D. Hybrid S/CS List-mode EM Algorithm

We have found it very useful to investigate the possibility of combining the advantages of the S-LMEM and CS-LMEM algorithms into a hybrid algorithm. Namely, one typically notices, as also shown in Sec. V, that the regular S-LMEM algorithm, in the first few subsets, is able to produce images of higher quality relative to the CS-LMEM algorithm, whereas the latter is able to exhibit convergent resolution and contrast behavior as the iterations proceed. The hybrid approach we have taken uses S-LMEM for the entire or part of the first iteration, followed by CS-LMEM in the rest of the calculation.

III. LIST-MODE PROJECTION TECHNIQUES

In general, forward- and back-projection schemes can be performed using two main approaches: voxel-driven and LOR-driven. It has been suggested [14]–[16] that best results may be obtained when the back- and forward-projection operations are *output driven*: i.e. if back-projecting, the process should be voxel-driven and if forward-projecting, the process should be LOR-driven. This has been explained by Wallis and Miller [15]. One simple way to see this is to note that if a projection is output driven, the operation would be a “many to one” operation rather than a “one to many” value operation. For instance, when back-projecting, an LOR-driven approach measures how each LOR contributes to all the voxels (“one to many”), whereas in the voxel-driven approach, one would be measuring the contributions of all the LORs to a given voxel at a time (“many to one”).

Nevertheless, due to the intrinsically LOR-based nature of list-mode reconstruction, only the LOR-driven projection operations may be utilized. This is one limitation of list-mode reconstruction, and is in a sense acquired due to the fact that one does not need to access the entire projection-space in list-mode reconstruction (which is one important potential advantage of the technique in the first place, especially for low-statistic frames in high resolution PET). Nevertheless, in our reconstructions, as shown later, we have *not* observed a degradation in image quality when switching from voxel-driven back-projection (used in histogram-mode) to LOR-driven back-projection.

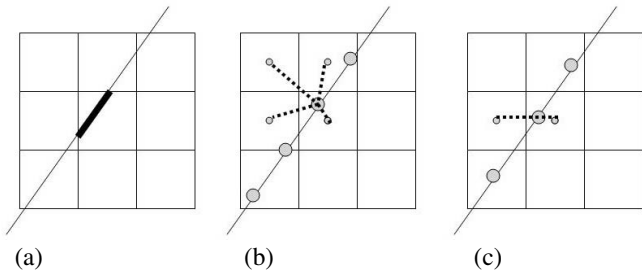


Fig. 1. Projection algorithms employing (a) the Siddon method, (b) trilinear, and (c) bilinear interpolation techniques are drawn, as elaborated in text.

Three LOR-driven projection techniques were explored for use in list-mode reconstruction:

1) *The Siddon method*: Following work of Siddon [17], this technique is based on calculating the path length of intersection of a given LOR along each voxel, as depicted in Fig. (1a).

2) *Trilinear interpolation*: To understand this technique, let us consider an image grid with voxels of unit length in all directions. Trilinear interpolation works by stepping through a given LOR with increments of unit length, as shown in Fig. (1b) for the 2D case. For back-projection then, one distributes the LOR value between the nearest voxels (four in 2D, eight in 3D). In forward projection similarly, the LOR value is obtained from the nearest eight (four) voxels in 3D (2D).

3) *Bilinear interpolation*: In bilinear interpolation, the length of increments on a given LOR is chosen so as to ensure that the sampled points lie along the centers of the voxels in one direction, in order to eliminate interpolation in that direction. In our case, the dimension along which interpolation is eliminated is the transaxial (X or Y) direction along which the given LOR increases faster; e.g. Y direction for the LOR shown in Fig. (1c). This method is potentially less accurate (which we have *not* observed to be the case, as shown later) than the trilinear counter-part since it makes the lengths of the increments LOR-dependent. However, the technique is faster since: (i) interpolation along one direction is eliminated; i.e. for each point on the LOR, an interpolation is performed over only four (two) nearest voxels in 3D (2D), and (ii) for oblique LORs, less number of samples per LOR are considered.

IV. METHODS

Tomograph: Data were acquired on the second generation of the high resolution research tomographs (HRRT). This HRRT scanner has an octagonal design, with the detector heads consisting of a double 10 mm layer of LSO/LYSO for a total of 119,808 detector crystals (crystal size 2.1 x 2.1 x 10 mm³). The total number of possible LORs is 4.486x10⁹.

Phantoms used and measurements performed: Using a technique [18] which allows printing of radioactive patterns using a modified standard ink-jet printer, we imaged radioactive (¹⁸F) point sources of size 0.7 mm placed at X=0,1,2,3,4,5 and 6 cm radially away from the center of the FOV. The sample also included a 1x7 cm rectangular area of uniform activity created for the purpose of monitoring noise behavior.

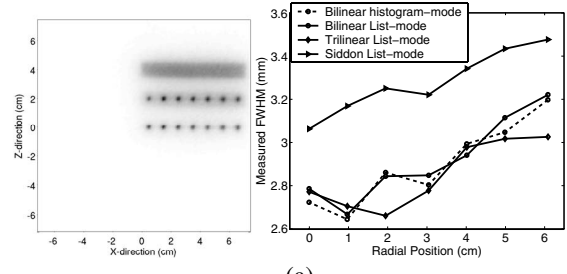


Fig. 2. (a) A sample reconstruction of the radioactive paper source (3 iterations of the S-LMEM algorithm). The lower row of points sources as well as the rectangular box were utilized for analysis of resolution and noise properties. (b) Plots of FWHM using various projection techniques: the bilinear and trilinear methods work noticeably better than the Siddon method.

For better visualization, a sample reconstructed image of the radioactive paper source is shown in Fig. (2a). The middle row of point sources (which were printed over a background were not utilized for analysis in this work.

The overall FWHM for any given point was measured by calculation of the root mean squared value of the measured point widths in the transaxial (X,Y) and axial (Z) directions. The percentage noise (standard deviation/mean) for a given reconstructed image was calculated in two ways:

- 1) *Voxel noise*: in which percentage variation of the individual voxels along the entire rectangle was measured.
- 2) *ROI noise*: in which the activity rectangle was sub-divided into eight small rectangular ROIs, and the percentage variation of the sum of counts in the ROIs was measured.

In all the reconstructions, 16 subsets were used for the accelerated algorithms. The hybrid S/CS-LMEM algorithm consisted of having the first 8 subsets being iterated using the S-LMEM approach and subsequently switching to the CS-LMEM counterpart. The following experiments and analyses were performed:

i) Comparison of Projection Techniques: Three LOR-driven projection methods were implemented in list-mode EM reconstruction: (a) the Siddon method as well as (b) trilinear and (c) bilinear interpolation techniques. Histogram-mode EM reconstruction was also applied to the data for comparison purposes (d) wherein output driven bilinear interpolation (i.e. voxel-driven back-projection and LOR-driven forward-projection) was employed, as recommended by previous investigators (see discussion in Sec. III). Three iterations of the S-LMEM algorithm (cases (a),(b), and (c)) and the OSEM algorithm (case (d)) were performed. Subsequently, the resolution (FWHM) and noise properties of the reconstructed images were compared.

ii) Convergent List-mode Reconstruction: We next studied convergent list-mode reconstruction algorithms. We performed the following comparisons (for cases when (i) Siddon and (ii) bilinear interpolation techniques were used):

(a) plots of measured FWHM vs. iteration (for two selected point sources 1 and 5 cm away from the center of the FOV) were calculated and shown for three iterations of the 3D-OSEM, S-LMEM, CS-LMEM and and hybrid S/CS-LMEM

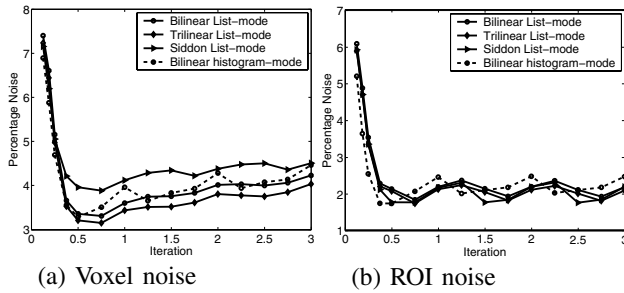


Fig. 3. Plots of noise vs. iteration for various projection techniques.

reconstruction schemes.

(b) Plots of measured FWHM vs. radial position were also depicted for these four schemes to compare the final reconstructed FWHM values across the FOV.

(c) Plots of noise vs. iteration were also calculated for the 3D-OSEM, S-LMEM, CS-LMEM and hybrid S/CS-LMEM reconstruction schemes.

V. RESULTS AND DISCUSSION

i) Comparison of Projection Techniques:

Fig. (2b) shows measured resolution values for the various points across the FOV, upon application of three iterations of the S-LMEM algorithm to the data. For comparison, results of application of histogram-mode EM reconstruction are also shown, wherein voxel-driven back-projection and LOR-driven forward-projection (referred to as output-driven projection) were used.

Note that one is also able to observe space-variance of the point spread function. This effect occurs due to a higher probability of inter-crystal penetration with higher angles of radiation incident on crystal fronts. Depth-of-Interaction (DOI) encoding has improved this problem, but has not reached complete space-invariance. In [19], we have presented a practical *ad hoc* approach to model the space-variance and anisotropy of the point-spread function into the system matrix of the EM algorithm for the HRRT.

Similarly, noise vs. iteration plots are shown in Fig. (3) for the aforementioned reconstruction algorithms, wherein (a) voxel-noise and (b) ROI-noise were considered, as described in the methods section. Three main observations can be made with respect to these figures:

- 1) Clearly, the Siddon technique performs noticeably poorly compared to the other reconstruction algorithms (especially in terms of resolution).
- 2) Trilinear and bilinear interpolation techniques perform nearly similarly.
- 3) Histogram-mode reconstruction with output-driven projections does not perform better than list-mode reconstruction with LOR-driven projections.

The current implementation of the trilinear interpolation technique is $>3-4$ times slower than the Siddon method, while Bilinear interpolation is comparable to the latter (only around 20% slower). This has therefore given us sufficient motivation

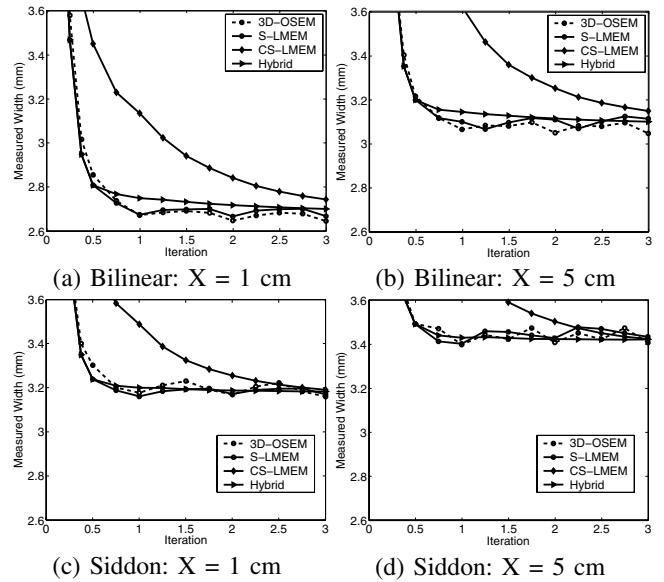


Fig. 4. Plots of reconstructed FWHM vs. iteration are shown for the 3D-OSEM, S-LMEM, and the CS-LMEM and hybrid algorithms for the point source located at 1 cm and 5 cm from center of the FOV.

to perform our reconstructions using projection algorithms which employ bilinear interpolation.

ii) *Convergent List-mode Reconstruction:* Figs. (4a,b) show plots of reconstructed FWHM width vs. iteration for point sources located at $X=1$ cm and 5 cm from center of FOV, with the data reconstructed using the 3D-OSEM, S-LMEM, CS-LMEM and hybrid S/CS-LMEM algorithms. Bilinear interpolation was used in the projection algorithms.

The values of FWHM resolution are seen to change in a cyclical manner for the 3D-OSEM and S-LMEM algorithms. In Fig. (4a), for instance, the FWHM width reconstructed using the S-LMEM approach is seen to oscillate between a low of 3.17 and a high of 3.23mm. Nevertheless, one clearly observes that in the CS-LMEM approach, due to its converging behavior, the FWHM widths improve with further iterations in a systematic and predictable manner.

One is also able to observe that the hybrid approach results in a faster decrease in reconstructed FWHM width with less iterations while maintaining the non-cyclical behavior. For comparison purposes, similar plots are shown when using the Siddon method, as seen in Figs. (4c,d). Clearly, bilinear interpolation is seen to result in superior image qualities.

Fig. (5) shows plots of measured FWHM values after three iterations for all the seven points located at $X=0,1,2,3,4,5$ and 6 cm from the center of FOV. We note from the plots that the histogram-mode and list-mode algorithms are able to achieve nearly similar FWHM values for a given point. Results when applying the (a) bilinear and (b) Siddon methods are shown. The bilinear interpolation method is seen to outperform the Siddon technique for all the point sources. Furthermore, we note that the convergent and hybrid techniques perform at least as well as (if not better than) the regularly subsetted list-mode

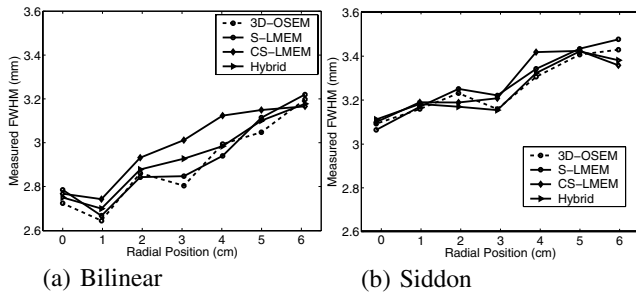


Fig. 5. Plots of reconstructed FWHM vs. radial position are shown for the 3D-OSEM, S-LMEM, and the CS-LMEM and hybrid algorithms. Three iterations were used.

and histogram-mode EM algorithms.

Noise vs. iteration plots are shown in Fig. (6) for the aforementioned reconstruction algorithms (using the bilinear technique), wherein (a) voxel-noise and (b) ROI-noise were considered. The convergent CS-LMEM algorithm lowers noise levels more slowly, compared to the other algorithms, and after the first iteration still exhibits higher values. On the other hand, the hybrid algorithm is seen to be suitable for reconstructions where early termination is used (for time-cost considerations) as it reaches noise levels comparable to (and possibly, voxel-wise, better than) other non-convergent algorithms.

VI. CONCLUSION

Three LOR-driven projection techniques were considered: (a) the Siddon method as well as (b) trilinear and (c) bilinear interpolation methods. We were able to demonstrate that the Siddon approach performs poorly compared to the other two algorithms (especially in terms of FWHM). Our method of choice was therefore the bilinear approach as it was considerably faster than the trilinear interpolation technique and produced comparable image qualities.

Using regular subsetized list-mode reconstruction, we were able to observe limit cycles: oscillatory alternations in image quality parameters with further subsets and iterations into the data. To address this issue, we implemented a convergent list-mode EM reconstruction algorithm, based on previous work [1]–[3], and investigated its properties using experimental PET data. It was demonstrated that the algorithm is robust and does not result in limit cycles.

A hybrid algorithm was also proposed, and was shown to combine the advantages of the the ordinary and the convergent list-mode algorithms (i.e. it was able to reach a higher image quality in less number of iterations while maintaining a convergent behavior), making it a good alternative to the ordinary subsetized list-mode EM algorithm.

REFERENCES

- [1] I. T. Hsiao, A. Rangarajan, and G. Gindi, "A provably convergent OS-EM like reconstruction algorithm for emission tomography", *Conf. Rec. SPIE Med. Imaging*, vol. 4684, pp. 10-19, 2002.
- [2] I. T. Hsiao, A. Rangarajan, and G. Gindi, "A new convergent MAP reconstruction algorithm for emission tomography using ordered subsets and separable surrogates", *Conf. Rec. IEEE Int. Symp. Biomed. Imaging*, pp. 409-412, 2002.

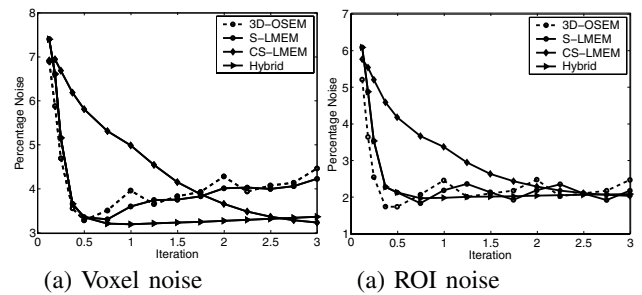


Fig. 6. Plots of noise vs. iteration are shown for the 3D-OSEM, S-LMEM, and the CS-LMEM and hybrid algorithms. Three iterations were used.

- [3] P. K. Khurd and G. R. Gindi, "A Globally Convergent Ordered-Subset Algorithm for List-Mode Reconstruction", *IEEE NSS & MIC 2003 conf. rec.*, Portland, OR, Oct 2003.
- [4] H. M. Hudson and R. S. Larkin, "Accelerated image reconstruction using ordered subsets of projection data", *IEEE Trans. Med. Imag.*, vol. 13, no. 4, pp. 601-609, 1994.
- [5] C. Byrne, "Accelerating the EMML Algorithm and Related Iterative Algorithms by Rescaled Block-Iterative Methods", *IEEE Trans. Imag. Process.*, vol. 7, pp. 100-109, 1998.
- [6] C. Byrne, "Likelihood Maximization for List-Mode Emission Tomographic Image Reconstruction", *IEEE Trans. Med. Imag.*, vol. 20, pp. 1084-1092, 2001.
- [7] H. Erdoğan and J. A. Fessler, "Ordered subsets algorithms for transmission tomography", *Phys. Med. Biol.*, vol. 44, pp. 2835-2851, 1999.
- [8] A. J. Reader *et al.*, "Fast accurate iterative reconstruction for low-statistics positron volume imaging", *Phys. Med. Biol.*, vol. 43, pp. 835-846, 1998.
- [9] A. J. Reader *et al.*, "One-Pass List-Mode EM Algorithm for High-Resolution 3-D PET Image Reconstruction Into Large Arrays", *IEEE Trans. Nucl. Sci.* vol. 49, pp. 693-699, 2002.
- [10] J. Browne and A. De Pierro, "A row-action alternative to the EM algorithm for maximizing likelihoods in emission tomography", *IEEE Trans. Med. Imag.*, vol. 15, no. 5, pp. 687-699, 1996
- [11] A. R. De Pierro and M. E. B. Yamagishi, "Fast EM-like methods for maximum *a posteriori* estimates in emission tomography", *IEEE Trans. Med. Imag.*, vol. 20, no. 4, pp. 280-288, 2001
- [12] S. Ahn and J. Fessler, "Globally convergent ordered subsets algorithms for emission tomography using relaxed ordered subsets algorithms", *IEEE Trans. Med. Imag.*, vol. 22, no. 5, pp. 613-626, 2003.
- [13] L. Parra and H. H. Barrett, "List-mode Likelihood: EM algorithm and image quality estimation demonstrated on 2-D PET", *IEEE Trans. Med. Imag.*, vol. 17, no. 2, pp. 228-235, 1998.
- [14] M. Egger, "Fast volume reconstruction in positron emission tomography: implementation of four algorithms on a high performance scalable parallel platform", *Ph.D. thesis*, University of Lausanne, Switzerland, 1996.
- [15] J. W. Wallis and T. R. Miller, "An Optimal Rotator for Iterative Reconstruction", *IEEE Trans. Med. Imag.*, vol. 16, pp. 118-123, 1997.
- [16] A. J. Reader, "Image Reconstruction and Correction Techniques for Positron Volume Imaging with Rotating Planar Detectors", *Ph.D Thesis*, University of London, 1999.
- [17] R. L. Siddon, "Fast calculation of the exact radiological path for a three-dimensional CT array", *Med. Phys.*, vol. 12, pp. 252-255, 1985.
- [18] V. Sossi, K. R. Buckley, P. Piccioni, A. Rahmim, M-L. Camborde, S. Lapi, and T. J. Ruth, "Printed sources for positron emission tomography (PET)", *IEEE Trans. Nucl. Sci.*, In Print, 2004.
- [19] A. Rahmim, M. Lenox, C. Michel, A. J. Reader, and V. Sossi, "Space-Variant and Anisotropic Resolution Modeling in List-Mode EM Reconstruction", *IEEE Med. Imag. Conf. Record*, Nov 2003.